Depth of the 660-km discontinuity near the Mariana slab from an array of ocean bottom seismographs

Rigobert Tibi,[1] Douglas A. Wiens,[1] Hajime Shiobara,[2] Hiroko Sugioka,[3] and Patrick J. Shore[1]

Received 1 September 2005; revised 2 December 2005; accepted 15 December 2005; published 26 January 2006.

[1] High frequency records of deep Mariana earthquakes from a dense array of ocean bottom seismographs deployed in the Mariana arc and back-arc regions are stacked and searched for the phases *P*660*p* and *S*660*p* to constrain the depth of the 660-km discontinuity near the Mariana slab. Results of the high-resolution study suggest that around 18°N the 660-km discontinuity lies at about 710–730 km (±14 km) depth within or in the vicinity of the slab core. In the region seismicity ceases at ~620 km depth. This implies that, although tomographic images show the Mariana slab penetrating into the lower mantle, deep seismicity in the region terminates ~100 km above the base of the transition zone. These findings and similar observations in Tonga argue that factors other than the phase transition at the base of the upper mantle may control the maximum down-dip extent of the deep seismogenic region in the slab. **Citation:** Tibi, R., D. A. Wiens, H. Shiobara, H. Sugioka, and P. J. Shore (2006), Depth of the 660-km discontinuity near the Mariana slab from an array of ocean bottom seismographs, *Geophys. Res. Lett.*, *33*, L02313, doi:10.1029/2005GL024523.

1. Introduction

[2] The nature of the 660-km discontinuity, separating the upper from the lower mantle, has important implications for mantle dynamics. It is widely accepted that the discontinuity is associated with the phase transformation from ringwoodite to perovskite + magnesiowüstite [e.g., *Ringwood*, 1969]. This idea is compatible with a single-layer convective mantle, in contrast to a compositional change that would separate the mantle into two convection regimes [e.g., *Christensen and Yuen*, 1984]. The ringwoodite to post-spinel phase transition possesses a negative Clapeyron slope. Hence, the elevation of the 660-km discontinuity should be depressed by the lower temperatures associated with subducting slabs.

[3] It is generally assumed that for deep-reaching subduction zones the maximum deep extent of seismicity is controlled by the depth of the 660-km discontinuity [e.g., *Green and Zhou*, 1996; *Okal and Bina*, 1998]. Several reasons why deep earthquakes would be completely inhibited below the 660-km discontinuity have been proposed. *Green and Zhou* [1996] suggested, in the context of transformational faulting model that deep earthquakes cannot be associated with an endothermic phase transition such as the 660-km discontinuity. *Karato et al.* [2001] proposed that the phase change at 660 km depth results in extremely fine-grained weak material below the 660-km discontinuity. This material would be incapable of supporting the ductile shear zone mechanism he favors for deep earthquakes. Indeed, if earthquakes are inhibited at precisely the 660-km discontinuity depth, this provides strong constraints on the mechanism of deep earthquakes and perhaps the rheology of mid-mantle.

[4] In this study, we use data of Mariana deep earthquakes recorded during the recent US and Japanese deployment of ocean bottom seismographs (OBS) and land stations in Mariana to determine the depths of the 660-km discontinuity near the Mariana slab. Compared to teleseismic studies, the short path lengths for the local data provide high frequency content and smaller Fresnel zones for precise determination of the 660 structure. The asserted relationship between the maximum depth extent of seismicity and the depth of the 660-km discontinuity is investigated.

2. Data

[5] From June 2003 to May 2004, US and Japanese institutions deployed 58 ocean bottom seismographs throughout the Mariana subduction zone region. The 50 US OBSs were equipped with three component L-4 sensors and amplifiers that extended their recording out to approximately 100 s period giving them a semi-broadband response, and the 8 Japanese OBSs were equipped with three component semi-broadband Precision Measuring Devices sensors. During the same time period, 20 broadband PASSCAL land stations were operated on 10 Mariana islands (Figure 1). A total of 70 sensors returned usable data. Both the seafloor and land deployments were parts of the MARGINS Subduction Factory experiment of the Mariana system.

[6] A large number of OBSs were concentrated along a profile perpendicular to the island arc near 18° north (Figure 1). We stacked data of deep Mariana earthquakes recorded by this high-density array of OBSs, and searched for high-frequency reflected and/or converted phases from the 410 and 660-km discontinuities (*s*410*p*, *P*660*p* and *S*660*p*) arriving within the *P* wave coda (Figure 2). Four deep earthquakes with $m_b > 4.6$ generated high-quality data at the network. Two of them occurred within the first 40 days of the deployment, the time period during which most of the OBSs were operating. For these events, we divided the dense network into two sub-arrays A1 and A2

[1]Department of Earth and Planetary Sciences, Washington University, St. Louis, Missouri, USA.
[2]Earthquake Research Institute, University of Tokyo, Tokyo, Japan.
[3]Institute for Frontier Research on Earth Evolution, Independent Administrative Institution, Japan Agency for Marine-Earth Science and Technology, Yokosuka, Japan.

Copyright 2006 by the American Geophysical Union.
0094-8276/06/2005GL024523$05.00

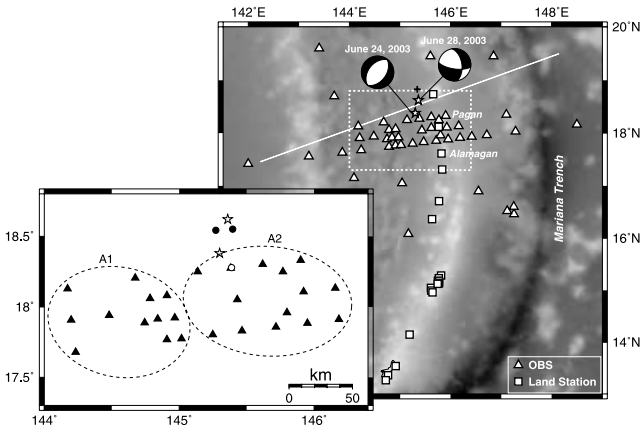

Figure 1. Map of the Mariana region showing the locations of the OBS sites (triangles) and island stations (squares). The locations (stars) and focal mechanism of the earthquakes used in this study are indicated (Table 1). The focal mechanism for the June 24, 2003 event is taken from the Harvard CMT solution. Cross indicates the location of the main shock in the deep 1995 Mariana sequence [*Tibi et al.*, 2001]. Solid line shows the location of the vertical cross section in Figure 5. Dashed rectangle delimits the area enlarged in the inset at the bottom left corner. Inset displays the locations of the OBS sites for the sub-arrays A1 and A2. Stars indicate the event locations. Open and solid circles are the locations of the interaction points at the 660-km discontinuity for *P*660*p* and *S*660*p*, respectively (Table 1).

of 12 and 14 elements, respectively (Figure 1). Apertures for the sub-arrays are 90 km × 60 km for A1, and 110 km × 60 km for A2. Division of the network into small aperture sub-arrays ensures that discontinuity phases recorded at the stations of each sub-array sample nearly the same structure, giving more coherency across the sub-array. For the two earthquakes that occurred later during the deployment period, the limited number of the operating OBSs would not allow adequate enhancement of the discontinuity phases for each individual sub-array. In addition, the high-frequency discontinuity phases would likely be incoherent across an array consisting of the entire network, given its relatively large aperture and the expected short-scale variations in discontinuity topography near the slab. Therefore, data recorded at 2 land stations and 5 OBSs, densely distributed in and around the islands of Pagan and Alamagan, were stacked and searched for the discontinuity phases in that case (Figure 1). Searches for *s*410*p* were unsuccessful for all the four events studied. Hence, the paper focusses only on the 660-km discontinuity.

3. Event Relocation and Focal Mechanism Determination

[7] In order to obtain high-precision locations, picked *P* and *S* arrival times from both land stations and OBSs (including those too distant to be included in the array analysis) were combined with global data provided by the Preliminary Determination of Epicenters to invert for the hypocenter of the earthquakes used in the investigation. Upgoing waves recorded by the local stations provided good control of the focal depths. The estimated maximum uncertainty in location is in the order of ±2 km. Parameters for the June 24 and 28, 2003 earthquakes are listed in Table 1. These events are those that occurred when the entire OBS network were operating, and their waveforms show clear 660 phases after stacking. For the remaining two events, namely the August 02 (m_b 4.7) and December 13, 2003 (m_b 4.8) earthquakes, we did not observe any discontinuity phase. Therefore, these events are not discussed further.

[8] A CMT solution is available for the June 24 event, but not for the June 28 earthquake. In order to predict amplitudes of discontinuity phases and compute theoretical seismograms for both events, we determined the focal mechanism for the June 28 earthquake using both local and teleseismic data in a grid search method that fits *P* and *S* waveforms simultaneously. The June 28, 2003 event is located only ∼10 km from, and within the depth range of about 570–600 km spanned by, the 1995 Mariana deep sequence [*Tibi et al.*, 2001]. The inferred focal mechanism for the June 28, 2003 earthquake (Figure 1) is similar to those of several aftershocks in the 1995 sequence. This similarity is further corroborated by polarities at regional stations, common to both the 2003 event and the 1995 sequence.

4. Array Analysis

[9] Vertical component seismograms for each event/array pair are deconvolved to ground displacement, resampled at 40 Hz and bandpass filtered at 0.5–5 Hz. *P* waveforms of 10 s length (starting from the *P* wave onset) are used to create a deconvolution filter, which is then applied to the seismograms to remove the earthquake source-time function, and water reverberations arriving few seconds after *P* onset. Seismograms are subsequently aligned on the maximum amplitude of the direct *P* pulse, as shown in Figure 3, and slant-stacked to reduce incoherent noise, and enhance discontinuity phases. We use an *N*th-root stacking algorithm ($N = 4$) [*Muirhead and Datt*, 1976], which is more efficient in noise reduction, and provides better time and slowness resolution, compared to linear stacking. A more detailed description of the array methodology is given by *Tibi and Wiens* [2005]. In order to assess the ability to

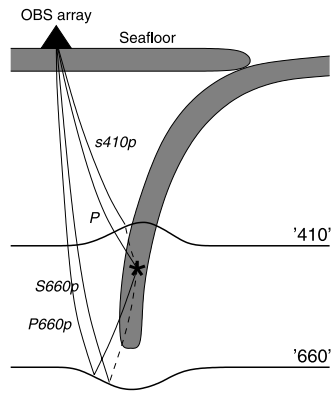

Figure 2. Schematic illustration of the ray paths for the different phases investigated. Solid and dashed lines indicate *P* and *S* path segments, respectively.

Table 1. Earthquakes and Interaction Depths[a]

Event	Date, YY MM DD	Origin Time, UT	Latitude, deg	Longitude, deg	Depth, km	Magnitude, m_b	Sub-Array	Observed Phase	R/C Lat, deg	R/C Lon, deg
1	03 06 24	04:30:58.5	18.38	145.30	523	4.9	A2	*P*706*p*	18.28	145.39
2	03 06 28	19:09:50.7	18.62	145.36	598	4.7	A1	*S*724*p*	18.54	145.27
							A2	*S*730*p*	18.55	145.40

[a]YY MM DD is year month, day; read 03 06 24 as 24 June 2003. R/C is the reflection and/or conversion point; Lat is latitude, and Lon is longitude.

infer the ray parameters using the sub-arrays A1 and A2, we computed their response functions in the frequency band of 0.5–5 Hz [*Rost and Thomas*, 2002], and estimated the slowness resolutions to be 0.05 to 0.2 sec/deg.

5. Results and Discussion

[10] Figure 4a shows a representative stack for the June 28, 2003 earthquake, as recorded at sub-array A1 (Table 1). In addition to the direct *P* wave, a secondary phase stands out clearly above the background noise. Its relative arrival time and slowness of ~33 sec and −0.7 (±0.2) sec/deg, respectively, are consistent with an *S* wave reflected and converted to *P* at about 724 km depth. A stack of synthetic waveforms computed for a 660-depth of 724 km, and processed the same way as the observed data corroborates this interpretation (Figure 4b). This phase was also detected by array A2, with a conversion depth of 730 km.

[11] Observed 660 phases with the estimated depths of the discontinuity for the different event/array pairs are indicated in Table 1. The inferred maximum uncertainty in the 660 depth estimates of ±14 km stems from three sources. (1) Owing to the high resolution provided by both the high-frequency data and fourth root stacking, phase picking errors are estimated to be not more than about ±0.3 sec. This translates to about ±3 km in discontinuity depth. (2) The estimated uncertainty in focal depth (discussed above) introduces about ±2 km of error in discontinuity depth. (3) Uncertainties from velocity model are largely associated with the slab anomaly. Above the event hypocenter, *P* and the discontinuity phases travel fairly similar paths. Hence, uncertainties introduced by inaccurate velocity model for that region are canceled out. The largest errors in 660 depths arise if the two-way paths of the discontinuity phase below the hypocenter occur entirely along the slab. Using the *Li and Romanowicz* [1996] slab velocity model, the apparent 660 depths would be about 6–9 km shallower than the actual depths for such scenario.

[12] The cross-section in Figure 5 shows that the *P*660*p* and *S*660*p* interaction points lie below the maximum depth of the seismogenic zone, but along or very close to its likely deep projection, suggesting that they are located within or in the near vicinity of the slab core. The inferred 660 depths of about 710–730 km (±14 km), which correspond to depression magnitudes of 50–70 km (relative to the global average depth), indicate the effect of the cold slab on the phase transition. Recent lower resolution analyses show

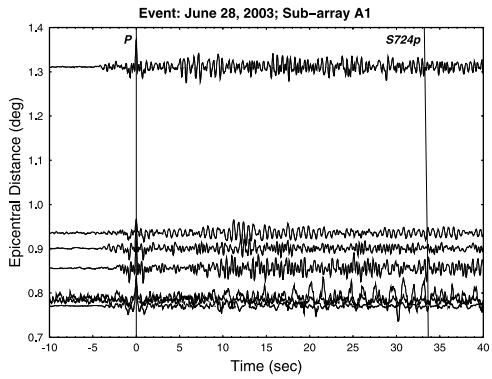

Figure 3. Seismic section for the June 28, 2003 earthquake (Table 1) and sub-array A1. The vertical component waveforms, which are aligned along the *P* pulse at time zero, were filtered with a bandpass of 0.5–5 Hz and deconvolved. Theoretical travel times predicted by a modified ak135 model for *S*724*p* (Figure 4a) are indicated. This phase is difficult to identify in individual traces due to the fact that its amplitudes are comparable to or below the noise level. However, the phase stands out clearly above the background noise after stacking (see Figure 4a).

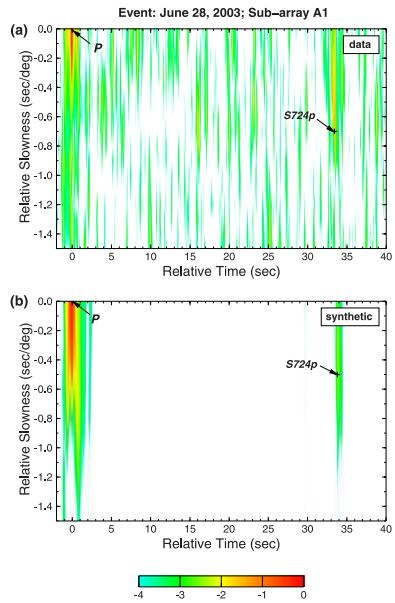

Figure 4. (a) Stack of the seismograms displayed in Figure 3. A fourth root stacking algorithm was used. Shown are the logarithms of the envelopes, calculated after normalizing the seismograms to the maximum amplitude of direct *P* pulse. Slowness and arrival time are relative to the direct *P* wave. An *S* wave reflected and converted to *P* at a depth of 724 km is marked with *S*724*p*. (b) Stack of theoretical seismograms calculated for a 660 depth of 724 km. Inaccuracies in the inferred focal mechanism lead to calculated *S*724*p* phase being weaker than in the observations.

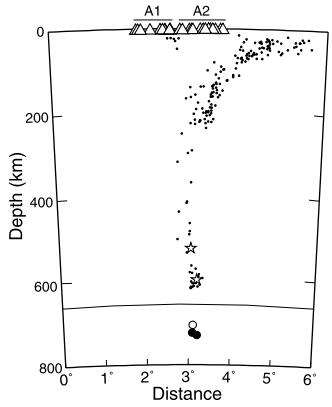

Figure 5. Vertical cross-section (see Figure 1) showing the locations of the earthquakes used (stars) and the interaction points at the 660-km discontinuity for *P*660*p* (open circle) and *S*660*p* (solid circles). Thin line indicates the depth of 660 km. Triangles are OBS sites for the sub-arrays A1 and A2. Seismicity (dots) from the *Engdahl et al.* [1998] catalog includes events within 200 km from the plane of the cross section. Note the ~100 km gap between the termination depth of the seismicity and the depths of the interaction points.

increasing 660 depths from about 670 km beneath the west Philippine basin to 700 km near the Mariana slab [*Suetsugu et al.*, 2003, 2005]. Discontinuity depths similar to those observed in this study have been reported for the Izu-Bonin subduction zone [*Wicks and Richards*, 1993], about 1000 km north of our study area, and parts of the Tonga and South America subduction zones [*Niu and Kawakatsu*, 1995; *Tibi and Wiens*, 2005; *Collier and Helffrich*, 2001].

[13] Around 18°N in Mariana, well-located deep seismicity terminates at ~620 km (±10 to 15 km) depth [*Engdahl et al.*, 1998], although tomographic imaging suggests that the slab does penetrate deep into the lower mantle [e.g., *van der Hilst et al.*, 1991]. Thus, the seismicity cutoff occurs about 90–110 km above the inferred base of the transition zone. Globally, reduction in seismic activity below 650 km is quite abrupt [*Stark and Frohlich*, 1985], and seismicity may not reach the base of the transition zone, given the observation that the discontinuity depth in cold subducting slabs is ~700 km. These facts indicate that factors other than the phase transition at the base of the upper mantle might control the maximum down-dip extent of the deep seismogenic region in the slab, contradicting earlier suggestions [*Green and Zhou*, 1996; *Okal and Bina*, 1998].

6. Conclusions

[14] We used high frequency data from deep Mariana earthquakes recorded by a local array of OBSs to constrain the depths of the 660-km discontinuity near the Mariana slab. Results suggest that around 18°N, the base of the upper mantle is located ~100 km below the deepest seismicity in the region. This and similar observations in Tonga seem to contradict an earlier assertion that the maximum down-dip extent of the deep seismogenic zone is controlled by ringwoodite to post-spinel phase transition at the base of the upper mantle.

[15] **Acknowledgments.** We thank the captain and crew of the R/V Kaiyo and R/V Wecoma for their effort in deploying and recovering the OBSs. The US OBSs were provided by the Lamont-Doherty Ocean Bottom Seismograph facility, and equipment for the land-based stations was provided by the PASSCAL program of the Incorporated Research Institutions for Seismology (IRIS). We also thank Juan Camacho and Joe Kaipat of the Saipan Emergency Management office for assistance in deploying the land seismographs. This research was financially supported through the MARGINS program under NSF grant OCE0001938.

References

Christensen, U. R., and D. A. Yuen (1984), The interaction of a subducting lithospheric slab with a chemical or phase boundary, *J. Geophys. Res.*, *89*, 4389–4402.

Collier, J. D., and G. R. Helffrich (2001), The thermal influence of the subducting slab beneath South America from 410 and 660 km discontinuity observations, *Geophys. J. Int.*, *147*, 319–329.

Engdahl, E. R., R. van der Hilst, and R. Buland (1998), Global teleseismic earthquake relocation with improved travel times and procedures for depth determination, *Bull. Seismol. Soc. Am.*, *88*, 722–743.

Green, H. W., and Y. Zhou (1996), Transformation-induced faulting requires an exothermic reaction and explains the cessation of earthquakes at the base of the mantle transition zone, *Tectonophysics*, *256*, 39–56.

Karato, S., M. R. Riedel, and D. A. Yuen (2001), Rheological structure and deformation of subducted slabs in the mantle transition zone: Implication for mantle circulation and deep earthquakes, *Phys. Earth Planet. Inter.*, *127*, 83–108.

Li, X.-D., and B. Romanowicz (1996), Global mantle shear-velocity model using nonlinear asymptotic coupling theory, *J. Geophys. Res.*, *101*, 22,245–22,272.

Muirhead, K. J., and R. Datt (1976), The *N*-th root process applied to seismic array data, *Geophys. J. R. Astron. Soc.*, *47*, 197–210.

Niu, F., and H. Kawakatsu (1995), Direct evidence for the undulation of the 660-km discontinuity beneath Tonga: Comparison of Japan and California array data, *Geophys. Res. Lett.*, *22*, 531–534.

Okal, E. A., and C. R. Bina (1998), On the cessation of seismicity at the base of the transition zone, *J. Seismol.*, *2*, 65–86.

Ringwood, A. E. (1969), Phase transformations in mantle, *Earth Planet. Sci. Lett.*, *5*, 401–412.

Rost, S., and C. Thomas (2002), Array seismology: Methods and applications, *Rev. Geophys.*, *40*(3), 1008, doi:10.1029/2000RG000100.

Stark, P. B., and C. Frohlich (1985), The depths of the deepest deep earthquakes, *J. Geophys. Res.*, *90*, 1859–1869.

Suetsugu, D., et al. (2003), Thick mantle transition zone beneath the Philippine Sea inferred using data from a long-term broadband ocean bottom seismograph array, paper presented at IUGG General Assembly, Int. Union of Geod. and Geophys., Sapporo, Japan.

Suetsugu, D., et al. (2005), Mantle discontinuity depths beneath the west Philippine basin from receiver function analysis of deep-sea borehole and seafloor broadband waveforms, *Bull. Seismol. Soc. Am.*, *95*, 1947–1956, doi:10.1785/0120040169.

Tibi, R., and D. A. Wiens (2005), Detailed structure and sharpness of upper mantle discontinuities in the Tonga subduction zone from regional broadband arrays, *J. Geophys. Res.*, *110*, B06313, doi:10.1029/2004JB003433.

Tibi, R., D. A. Wiens, and J. A. Hildebrand (2001), Aftershock locations and rupture characteristics of the 1995 Mariana deep earthquake, *Geophys. Res. Lett.*, *28*, 4311–4314.

van der Hilst, R., R. Engdahl, W. Spakman, and G. Nolet (1991), Tomographic imaging of subducted lithosphere below northwest Pacific island arcs, *Nature*, *353*, 37–43.

Wicks, C. W. J., and M. A. Richards (1993), A detailed map of the 660-kilometer discontinuity beneath the Izu-Bonin subduction zone, *Science*, *261*, 1424–1427.

H. Sugioka, Institute for Frontier Research on Earth Evolution, JAMSTEC, Natsushima-cho 2-15, Yokosuka, Kanagawa 237-0061, Japan.

H. Shiobara, Earthquake Research Institute, University of Tokyo, Yayoi 1-1-1, Tokyo, Bunkyo-ku 113-0032, Japan.

P. J. Shore, R. Tibi, and D. A. Wiens, Department of Earth and Planetary Sciences, Washington University, St. Louis, MO 63130, USA. (tibi@seismo.wustl.edu)